

Structural, electronic and vibrational properties of LaF₃ according to density functional theory and Raman spectroscopy

A S Oreshonkov^{1,2}, E M Roginskii³, A S Krylov¹, A A Ershov² and V N Voronov¹

¹ Kirensky Institute of Physics, Federal Research Center KSC SB RAS, Krasnoyarsk 660036, Russia

² Siberian Federal University, Krasnoyarsk 660079, Russia


³ Ioffe Institute, St. Petersburg 194021, Russia

E-mail: orshonkov@iph.krasn.ru

Abstract

Crystal structure of LaF₃ single crystal is refined in tysonite-type trigonal unit cell $P\bar{3}c1$ using density functional theory calculations and Raman spectroscopy. It is shown that trigonal structure with $P\bar{3}c1$ space group is more energy-efficient than hexagonal structure with space group $P6_3cm$. Simulated Raman spectra obtained using LDA approximation is in much better agreement with experimental data than that obtained with PBE and PBEsol functionals of GGA. The calculated frequency value of silent mode B_2 in case of hexagonal structure $P6_3cm$ was found to be imaginary (unstable mode), thus the energy surface obtains negative curvature with respect to the corresponding normal coordinates of the mode which leads to instability of the hexagonal structure in harmonic approximation. The A_{1g} line at 214 cm^{-1} in Raman spectra of LaF₃ related to the translation of F2 ions along c axis can be connected with F2 ionic conductivity.

Keywords: LaF₃, tysonite structure, DFT, electronic structure, lattice vibrations, Raman spectroscopy

 Supplementary material for this article is available [online](#)

(Some figures may appear in colour only in the online journal)

1. Introduction

LaF₃ is a well-known host for upconversion solid state materials doped with rare-earth ions [1, 2]. The optical properties of bulk LaF₃:Re³⁺ are investigated from the 1960s [3, 4] up to present [5]. The LaF₃ nanoparticles were synthesized from 2001 [6], and the nanocrystals doped with rare-earth ions— in 2002 [7]. The possibility of using Ce:LaF₃ as a UV laser material have been shown in the past [8, 9]. On the other hand, LaF₃ is known as a fast fluoride conductor at elevated temperatures [10, 11], and doping with Ba, Sr can improve the electronic conductivity of LaF₃ [11, 12].

From the beginning of the LaF₃ exploration, several works were devoted to structural analysis of this material and this

resulted in discrepancies concerning space group determination [13]. The crystal structure was described in tysonite trigonal form (space group $P\bar{3}c1$) [14, 15], figure 1(a), and in a hexagonal form (space group $P6_3cm$) [16, 17], figure 1(b).

The relationship between thermal vibrations and the fluoride ionic conductivity in the case of trigonal structure is discussed in [18]. It has been shown that ionic current parallel to c axis is predominantly carried by F2 and F3 fluorine ions moving, but ionic conduction perpendicular to c axis involves all fluorine sublattices.

The high pressure phase stability of LaF₃ up to 40 GPa was studied using density functional theory (DFT) calculations in WIEN2K [19] and up to 30 GPa in CASTEP [20] code. The initial structure was taken as a tysonite. The evolutionary

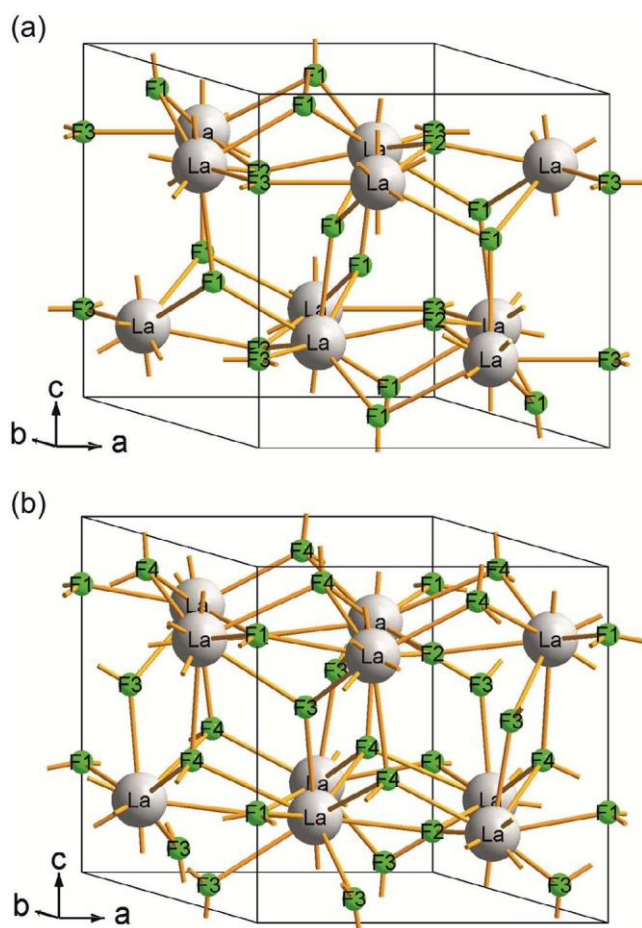


Figure 1. Trigonal (a) and hexagonal (b) structures of LaF_3 .

structure search method implemented in the USPEX code [21] in conjunction with density functional theory based *ab initio* band structure calculations method implemented in VASP code was used to predict crystal structure of LaF_3 up to 200 GPa [22].

In the present paper, the density functional theory and Raman spectroscopy methods are used for elimination of the discrepancy in the structure investigation results. The phonon wavenumbers and forms of Raman-active vibrations are calculated for the first time.

2. Experimental characterization

The unpolarized Raman spectra were collected in a backscattering geometry, using a triple monochromator Horiba Jobin Yvon T64000 Raman spectrometer operating in double subtractive mode, and detected by a LN-cooled charge-coupled device [23–25]. The single-mode argon line at 488 nm from a Spectra-Physics Stabilite 2017 Ar^+ laser of 7 mW on the sample was used as an excitation light source. The intensity of the laser light was adjusted to avoid sample heating.

Temperature measurements were carried out using a closed cycle ARS CS204-X1.SS helium cryostat in the temperature range of 7–400 K. The temperature was monitored by using a LakeShore DT-6SD1.4L silicon diode. During the experiments, the cryostat was evacuated to 10^{-6} mbar. The CCD

pixel coverage in an additive dispersion mode was as fine as 0.3 cm^{-1} , but it was limited by the spectrometer spectral resolution of 1.8 cm^{-1} .

The temperature experiments were carried out in a dynamic mode [26, 27] varying the sample temperature at the rate of 0.7 K min^{-1} . The uncertainty of the measured temperature for a given rate can be estimated as the difference between the adjacent measurements and it was $\pm 0.35 \text{ K}$ in one spectrum measurement. The overall time for a single spectrum accumulation was within 40 s. The spectra were acquired with a temperature step of 0.7 K.

3. Calculations

All the structural optimization, energy and Raman calculation were carried out by the CASTEP code [28] using the density-functional theory. The initial structures of LaF_3 with the space

group $P\bar{3}c1$ [15] and $P63cm$ [29] were fully optimized using the local density approximation (LDA) provided by the Perdew and Zunger [30] parameterization of the numerical results of Ceperley and Alder (CA-PZ) [31], Perdew–Burke–Ernzerhof (PBE) [32] and PBEsol (a version of the PBE functional that improves equilibrium properties of densely packed solids and their surfaces) [33] gradient-corrected functionals.

The calculations were performed using ultrasoft pseudopotentials with $5s^2 5p^6 5d^1 6s^2$ electrons for La atom and $2s^2 2p^5$ electrons for F atom treated as valence ones. The self-consistent field (SCF) procedure was used with a convergence threshold of $5.0 \cdot 10^{-9} \text{ eV/atom}$. The total energy was corrected for finite basis set with 3 cut-off energies. Geometry optimizations were performed with a convergence threshold of 0.01 eV \AA^{-1} on the max force, 0.02 GPa on the max stress, and 0.0005 Å on the max displacement. The energy cutoff was set to be 1000 eV, and the Brillouin zone was sampled by $4 \times 4 \times 3$ k -points for both structures using the Monkhorst–Pack scheme [34]. The phonon spectra at Γ point was calculated within harmonic approximation by diagonalization of hessian matrix calculated with finite displacement method. Then the eigenvalues and eigenvectors of hessian matrix was found with physical meaning of eigenvalues as squared harmonic frequencies and eigenvectors are normal coordinates of phonons [35, 36].

4. Results and discussion

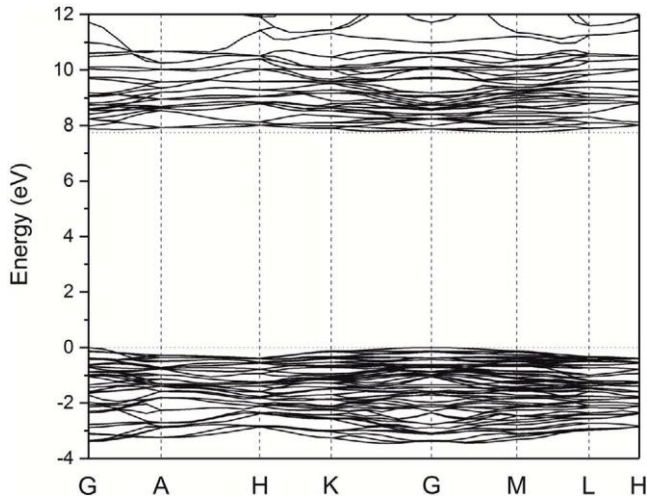
In order to analyze LaF_3 crystal, the optimization of initial structures was performed using local density approximation and gradient-corrected functionals PBE and PBEsol. The obtained crystallographic data in comparison with earlier published ones are shown in table 1. The cell parameters simulated in LDA underestimates experimental ones, while GGA (PBE) commonly overestimates cell parameters and this is in agreement to general tendency [37]. The results obtained within GGA PBEsol approximation are the most close relation to the experimental data. The final total energy obtained after geometry optimization for both trigonal and hexagonal structures are presented in table 2. In all cases, the trigonal phase is more energy profitable than hexagonal.

Table 1. Optimized structural parameters for $P3\ c1$ and $P63cm$ phases in comparison with experimental data.

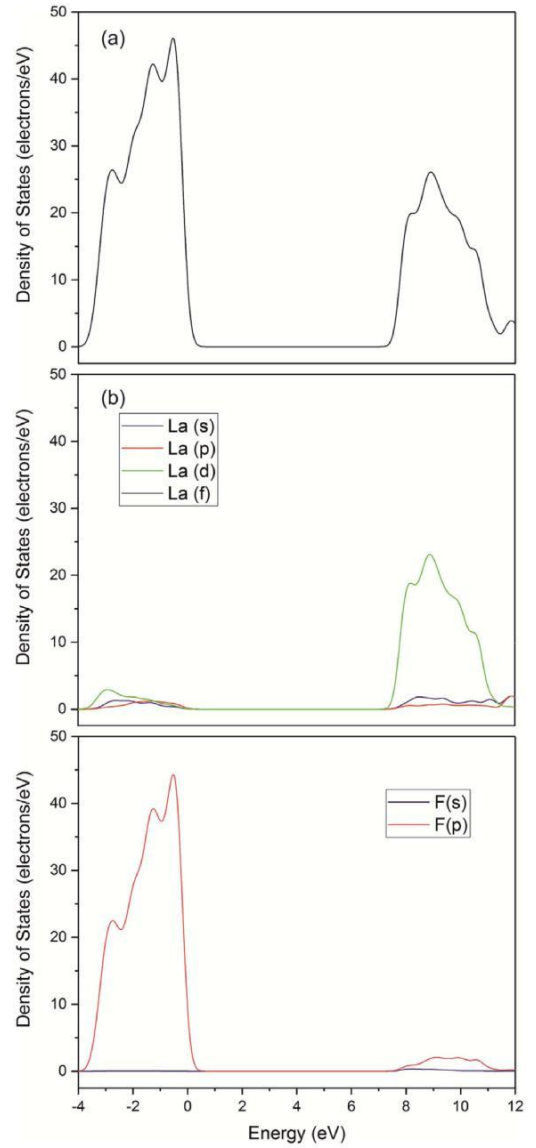
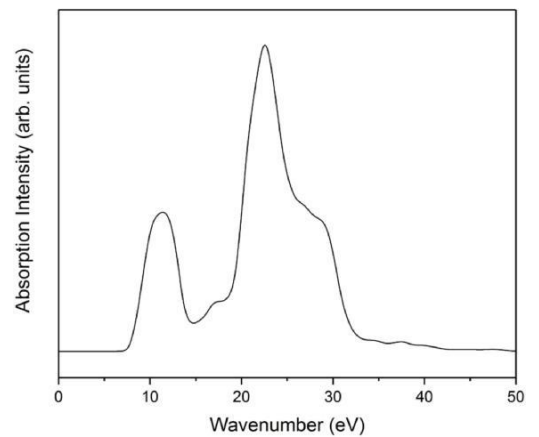
	LDA	PBE	PBESol	Exp [15]
a (Å)	7.104	7.317	7.206	7.185
c (Å)	7.305	7.495	7.403	7.351
	LDA	PBE	PBESol	Exp [29]
a (Å)	7.099	7.312	7.202	7.160
c (Å)	7.305	7.494	7.403	7.360

Table 2. Total energy (eV) of optimized LaF_3 structures.

	LDA	PBE	PBESol
Trigonal	-17 141.06	-17 150.90	-17 106.68
Hexagonal	-17 141.05	-17 150.88	-17 106.66
difference	0.01	0.02	0.02

**Figure 2.** Calculated band structure of LaF_3 .

The band structure of the trigonal LaF_3 structure obtained with the LDA method is plotted in figure 2. For the energy band calculations, the high-symmetry points of the BZ are selected as $G-A-H-K-G-M-L-H$. It is found that the valence band top is well localized in the vicinity of the G -point, the center of the Brillouin zone. The conduction band bottom is located at M -point (1/2,0,0). The band gap value for indirect electronic transitions is $E_g^i = 7.77$ eV. The direct band gap is located in the G -point of the Brillouin zone and the calculated band gap value of $E_g^d = 7.87$ eV. The difference between direct and indirect band gaps is insignificant and, thus, the LaF_3 is a wide band gap dielectric material. Comparing the obtained value $E_g = 7.87$ eV with experimental result of $E_g = 9.7$ eV [38], one may conclude that the DFT calculations in LDA approximation is slightly underestimate the experimental value that is common situation for DFT since the theory suffers from the well-known band gap underestimation problem. It has been noted [39] that the effective potential of the DFT is defined only with an additive constant which may depend on the total number of electrons in the system.

**Figure 3.** Total (a) and partial density of states (b) and (c) of LaF_3 .**Figure 4.** Calculated absorption spectrum of LaF_3 .

The variation of this constant when the electron number changes from N to $N + 1$ gives an additional contribution (the so-called ‘energy derivative discontinuity’) to the calculated value of the gap.

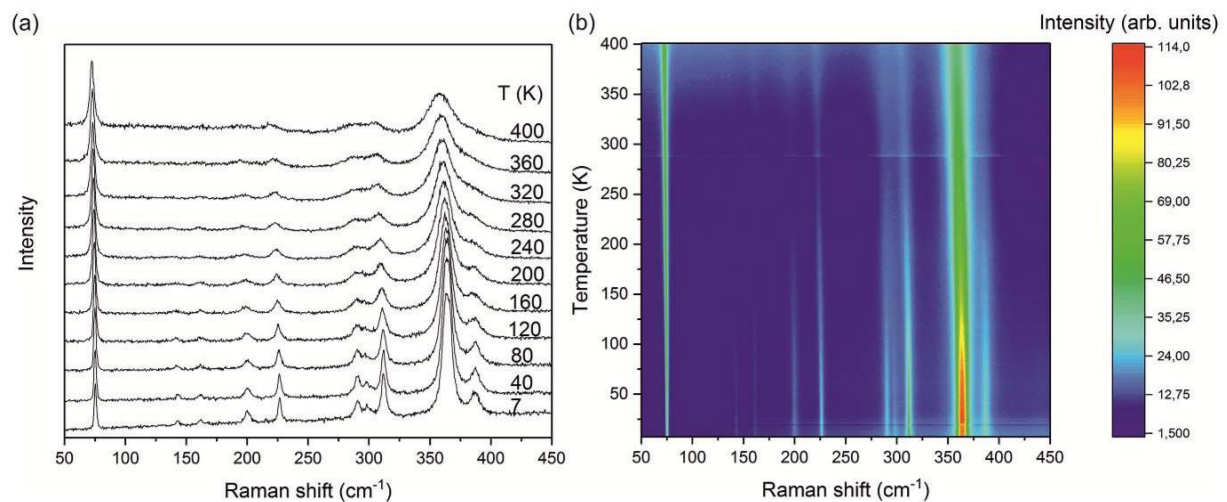


Figure 5. The temperature transformation of Raman spectra (a) and intensity map at temperatures 7–400 K (b).

The total and partial density of states of the trigonal LaF₃ structure obtained with the LDA method are shown in figure 3. As a result of the curve analysis, one can find that the valence band top is constructed mostly by p-electrons of F atoms while the conduction band bottom is constructed mostly by d-electrons of La atoms and, thus, La atoms obtain a configuration with completely empty d-orbital which is well correlated with experiment [38].

The absorption spectrum simulated with the LDA method using scissor operator (difference between the experimental and calculated E_g) equal to 1.83 eV is shown in figure 4. From the PDOS analysis (figure 3), it follows that the first peak is associated with electronic transitions mainly from the 2p orbitals of the F atom to the 5d orbitals of La atoms, while the second peak characterizes the transitions to the 6s and 5p orbitals of La atoms.

The temperature transformation and Intensity map of Raman spectra of LaF₃ are shown in figure 5. It is clearly seen, that spectral bands become narrower below 200 K and wider above 280 K, no significant changes related to structural phase transitions in the range of 7–400 K are observed.

–The vibrational representation for possible trigonal phase ($P\bar{3}c1$) at Brillouin zone center is $\Gamma_{\text{vibr}} = 5A_{1g} + 5A_{1u} + 7A_{2g} + 7A_{2u} + 12E_u + 12E_g$ where Raman active modes are $\Gamma_{\text{Raman}} = 5A_{1g} + 12E_g$ and for possible hexagonal phase at Brillouin zone center is $\Gamma_{\text{vibr}} = 8A_1 + 5A_2 + 5B_1 + 8B_2 + 13E_2 + 13E_1$ where Raman active modes are $\Gamma_{\text{Raman}} = 7A_1 + 13E_2 + 12E_1$. Thus, the Raman spectra of hexagonal structure should be more reach in lines than that of trigonal.

The calculation of vibrational properties has been carried out and simulated wavenumbers of Raman active modes in comparison of experimental spectra at 7 K are show in figure 6.

In both cases, there are no imaginary frequencies in Raman spectra of trigonal and hexagonal structures. However, there is an imaginary silent B_2 mode in hexagonal structure obtained with LDA, PBE and PBEsol approximations. Thus, hexagonal structure with $P63cm$ space group is unstable and only trigonal (tysonite, $P\bar{3}c1$ space group) structure can be appropriate for describing LaF₃ crystals.

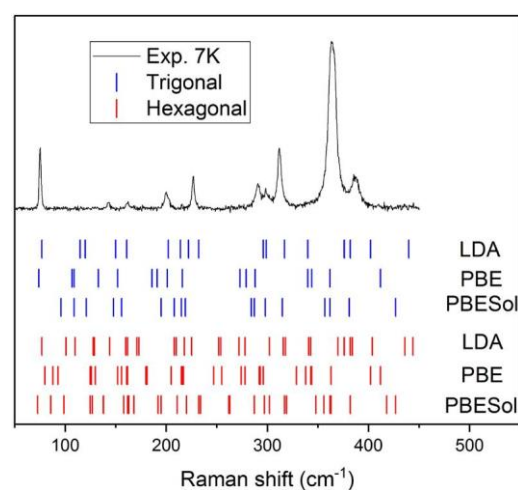


Figure 6. Comparison of experimental Raman spectra of LaF₃ at 7 K with results of LDA and GGA (PBE and PBEsol).

The calculations show that only one E_g Raman-active mode in the range of $<100\text{ cm}^{-1}$, should appear, that is in agreement with experimental data. This strong low-wavenumber band at 78 cm^{-1} is assigned to the vibration not only La ions, but the movement of the lanthanum and fluorine ion layers toward each other as shown in figure 7(a).

The A_{1g} line at 214 cm^{-1} is related to the translation of F₂ ions along c axis, as shown in figure 7(b), half of F₂ ions in unit cell moves up and half down. Such vibration can act as possible pathway for F₂ ion movement for explanation of ionic conductivity in LaF₃ that is in accordance with known model [18]. The next one active Raman line at 226 cm^{-1} is a similar vibration mixed translation of F₁, figure 6S (see supplementary data online at stacks.iop.org/JPhysCM/30/255901/mmedia). The Raman line at 312 cm^{-1} is a La–F₁,F₂ asymmetric stretching vibration (figure 7(c)) and the calculated wavenumber of La–F₃ asymmetric stretching is located is 340 cm^{-1} (figure 10S). The strong band around 365 cm^{-1} should contain two lines related to mixed vibration of F₁ and F₂ ions, as shown in figures 11S and 12S. The vibration related to the band at 387 cm^{-1} is shown in figure 7(d). In this case,

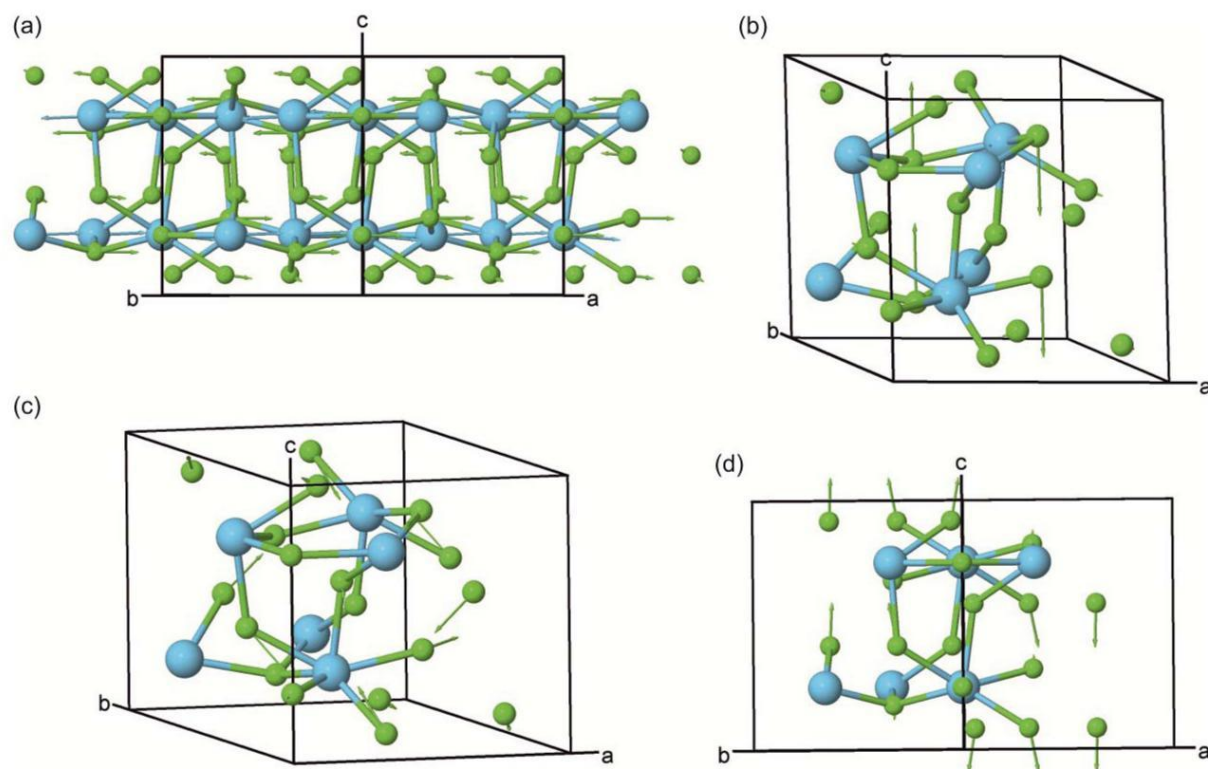


Figure 7. The lattice vibrations related to Raman lines at 78 cm^{-1} (a), 220 cm^{-1} (b), 312 cm^{-1} (c) and 387 cm^{-1} (d).

Table 3. Positions of the experimental Raman lines in comparison with the calculated ones for the trigonal structure obtained within local density approximation.

ω, cm^{-1} (exp)		ω, cm^{-1} (calc)		Mode assignment
300 K	7 K	A_{1g}	E_g	
73	75		78	LaF ₃ layers vibration
			116	La, F1
		120		F1, F2
135	142		151	La, F1
161	162		162	F1
196	200		202	F1
		214		F2 along <i>c</i> axis
223	226	222		F2 along <i>c</i> axis mixed with F1
			233	F1
		290	297	F1
289	298	299		F1
307	312		318	La—F1,2 asymm. stretching
			340	La—F3 asymm. stretching
360	362		377	F1, F2
	366		383	F1, F2
384	387	402		F1 along <i>c</i> axis
			445	F1, F2, F3 mixed vibration

half of F₁ ions moves up and half moves down. The modes assignment is presented in table 3 and the remaining lattice vibrations are depicted in figures 1S–13S.

5. Conclusions

The Raman spectra of LaF₃ were obtained in a wide range of temperatures (7–400 K). It was experimentally established

that the crystal structure is stable down to 7 K, which is consistent with the results of the first-principle calculations. The possible trigonal and hexagonal structures were calculated using LDA and GGA (PBE and PBEsol) approximations.

In all approximations, trigonal tysonite structure is more efficient in energy. In addition, an imaginary silent B_2 mode has been found in phonon spectra of hexagonal phase. Thus, it is shown that the LaF₃ structure can be described only in trigonal tysonite $P3^-c1$ space group.

The Raman line at 214 cm^{-1} (A_{1g}) attributed to the F2 ion movement along *c* axis can be used in an indicator during studying ionic conductivity in LaF₃.

Acknowledgments

The reported study was funded by RFBR according to the research project No. 17-52-53031 and 16-02-00102. It was partially supported by the Ministry of Education and Science of the Russian Federation and the ‘Krasnoyarsky regional fund of scientific support and scientific-technical activity’. The computations were performed using facilities of the Computational Centre of the Research Park of St. Petersburg State University.

ORCID iDs

A S Oreshonkov <https://orcid.org/0000-0003-3046-7018>

E M Roginskii <https://orcid.org/0000-0002-5627-5877>

A S Krylov <https://orcid.org/0000-0001-8949-0584>

References

- [1] Wang F and Liu X 2009 *Chem. Soc. Rev.* **38** 976–89
- [2] Haase M and Schfer H 2011 *Angew. Chem., Int. Ed.* **50** 5808
- [3] Hewes R A and Sarver J F 1969 *Phys. Rev.* **182** 427
- [4] Auzel F and Pecile D 1973 *J. Lumin.* **8** 32
- [5] Lorbeer C and Mudring A-V 2013 *J. Phys. Chem. C* **117** 12229
- [6] Zhou J, Wu Z, Zhang Z, Liu W and Dang H 2001 *Wear* **249** 333
- [7] Stouwdam J W and Van Veggel F C J M 2002 *Nano Lett.* **2** 733
- [8] Ehrlich D J, Moulton P F and Osgood R M 1980 *J. Opt. Lett.* **5** 339
- [9] Pedrini C, Moine B, Gacon J C and Jacquier B 1992 *J. Phys.: Condens. Matter* **4** 5461
- [10] Sher A, Solomon R, Lee K and Muller M W 1966 *Phys. Rev.* **144** 593
- [11] Sorokin N I and Sobolev B P 2007 *Crystallogr. Rep.* **52** 842
- [12] Roos A and Schoonman J 1984 *Solid State Ion.* **13** 205
- [13] Maximov B and Schulz H 1985 *Acta Cryst.* **B41** 88
- [14] Hudson P R W 1976 *J. Phys. C: Solid St. Phys.* **9** L39
- [15] Cheetham A K and Fender B E F 1976 *Acta Cryst.* **B32** 94
- [16] Gregson D, Catlow C R A, Chadwick A V, Lander G H, Cormack A N and Fender B E F 1983 *Acta Cryst.* **B39** 687
- [17] Afanasiev M L, Habuda S P and Lundin A G 1972 *Acta Cryst.* **B28** 2903
- [18] Belzner A, Schulz H and Heger G 1994 *Z. Krist.-Cryst. Mater.* **209** 239
- [19] Modak P, Verma A K, Ghosh S and Das G P 2009 *J. Phys. Chem. Solids* **70** 922
- [20] Winkler B, Knorr K and Milman V 2003 *J. Alloys Compd.* **349** 111
- [21] Glass C W, Oganov A R and Hansen N 2006 *Comput. Phys. Commun.* **175** 713
- [22] Sahoo B D, Joshi K D and Gupta S C 2017 *Indian J. Phys.* **91** 535
- [23] Atuchin V V, Aleksandrovsky A S, Chimitova O D, Gavrilova T A, Krylov A S, Molokeev M S, Oreshonkov A S, Bazarov B G and Bazarova J G 2014 *J. Phys. Chem. C* **118** 15404
- [24] Savina A A, Atuchin V V, Solodovnikov S F, Solodovnikova Z A, Krylov A S, Maximovskiy E A, Molokeev M S, Oreshonkov A S, Pugachev A M and Khaikina E G 2015 *J. Solid State Chem.* **225** 53
- [25] Atuchin V V, Subanakov A K, Aleksandrovsky A S, Bazarov B G, Bazarova J G, Gavrilova T A, Krylov A S, Molokeev M S, Oreshonkov A S and Stefanovich S Yu 2018 *Mater. Des.* **140** 488
- [26] Krylov A S, Kolesnikova E M, Isaenko L I, Krylova S N and Vtyurin A N 2014 *Cryst. Growth Des.* **14** 923
- [27] Moshkina E, Krylov A, Sofronova S, Gudim I and Temerov V 2016 *Cryst. Growth Des.* **16** 6915
- [28] Clark S J, Segall M D, Pickard C J, Hasnip P J, Probert M J, Refson K and Payne M C 2005 *Z. Kristallogr.* **220** 567
- [29] Rango C, Tsoucaris G and Zelwer C 1966 *C. R. Hebd. Seances Acad. Sci.* **263** 64
- [30] Perdew J P and Zunger A 1981 *Phys. Rev. B* **23** 5048
- [31] Ceperley D M and Alder B J 1980 *Phys. Rev. Lett.* **45** 566
- [32] Perdew J P, Burke K and Ernzerhof M 1996 *Phys. Rev. Lett.* **77** 3865
- [33] Perdew J P, Ruzsinszky A, Csonka G I, Vydrov O A, Scuseria G E, Constantin L A, Zhou X and Burke K 2008 *Phys. Rev. Lett.* **100** 136406
- [34] Monkhorst H J and Pack J D 1976 *Phys. Rev. B* **13** 5188
- [35] Refson K, Tulip P R and Clark S J 2006 *Phys. Rev. B* **73** 155114
- [36] Porezag D V and Pederson M R 1996 *Phys. Rev. B* **54** 7830
- [37] Haas P, Tran F and Blaha P 2009 *Phys. Rev. B* **79** 209902
- [38] Evarestov R A, Leko A V, Murin I V, Petrov A V and Veryazov V A 1992 *Phys. Status Solidi b* **170** 145
- [39] Perdew J P 1985 *Int. J. Quantum Chem.* **28** 497